Earthquake Geotechnical Engineering for Protection and Development of Environment and Constructions – Silvestri & Moraci (Eds)
© 2019 Associazione Geotecnica Italiana, Rome, Italy, ISBN 978-0-367-14328-2

Numerical analysis of inclined pile group performance in liquefiable sands

Y. Wang & R.P. Orense
The University of Auckland, Auckland, New Zealand

ABSTRACT: To investigate the performance of inclined piles on liquefiable ground during earthquakes, a three-dimensional finite element model has been developed using OpenSees program. The proposed modelling method takes account of the effects of soil-pile interaction and the dynamic behavior of liquefiable sand. The model suggested herein has been verified under monotonic pushover load at the pile head and seismic load at the model base. By changing the inclination angle of the pile and the amplitude of loading patterns, a series of parametric analyses is then conducted and the soil, cap and pile responses are compared. The results illustrate that the presence of inclined piles has a beneficial effect on the dynamic response of the soil-pile-cap system in non-liquefied soils. The occurrence of soil liquefaction with regard to cap response could still be beneficial. However, highly detrimental effects on the soil and pile responses could be observed as the soil liquefied.

1 INTRODUCTION

Inclined piles are widely applied in engineering practice to resist significant horizontal loadings under bridges and offshore constructions. However, the inadequate performance of inclined piles has been observed in various earthquakes. Pender (1993) listed several examples including the damaged Rio Banano Bridge during the 1991 Costa Rica earthquake and the wharf structures at the Port of Oakland in the 1989 Loma Prieta earthquake. The graphical design methods in early times were assumed to be the possible reason for the poor seismic performance of inclined piles. Gerolymos et al. (2008) summarized several drawbacks of inclined piles mentioned frequently in engineering practice, such as residual bending moment due to soil consolidation (pre-earthquake) and soil settlement (post-earthquake), tensile axial force along the pile, large kinematic force and undesirable rotation at the pile-cap connection.

Based on recent studies, the inclined pile has regained some popularity as its advantages have been highlighted in field studies, laboratory tests, as well as numerical investigations. Berrill et al. (2001) investigated the Landing Bridge after the 1987 Edgecumbe earthquake and found the effective impact of raked piles against lateral spreading. Zhang et al. (1999) carried out a series of centrifuge experiments for single batter piles subjected to lateral loads and observed an increase in lateral resistance for negatively inclined piles (battered forward against the lateral loading direction) and a decrease for positively inclined piles (battered reverse). As for laboratory tests (e.g. Dash & Bhattacharya 2015, Escoffier 2012, Li et al. 2016, McManus et al. 2005), most of the research is focused on dry sand or clay instead of liquefiable soils. Numerical models found in the literature (e.g. Ghorbani et al. 2014, Goit & Saitoh 2013, Wang & Orense 2014) are generally simplified without the consideration of soil plasticity or soil liquefaction. The influence of inclined piles on the dynamic behavior of the soul-pile system is still not well established.

This paper proposes a three dimensional finite element modelling method (3D FEM) through the platform of OpenSees (Mazzoni et al. 2007) developed by the Pacific Earthquake Engineering Research Center (PEER). The seismic behavior of the liquefiable soil is captured by the Pressure-Dependent Multi-Yield surface (PDMY02) material (Elgamal et al. 2003). The numerical model is firstly verified by predicting the pile behavior from two case studies. A parametric

analysis is then conducted to study the seismic response of the soil-pile system. Factors including the amplitude of input excitation and pile inclination have been investigated.

2 NUMERICAL MODEL DESCRIPTION

2.1 *Meshing and boundary conditions*

As shown in Figure 1, only half of the model was simulated because of symmetry. A pile with a diameter (or width) D and an inclination α was embedded in the soil block with total thickness $L\cos\alpha + 10D$, where L is the embedded length of the pile. Meshing around the pile was also different for piles with square (Figure 1b) or circle (Figure 1c) cross-sections. The model was meshed with solid-fluid coupled 8-node elements (Mazzoni et al. 2007). The soil elements were finer at sections closer to the pile, especially near the pile tip. All three translational displacements were fixed at the bottom of the model. The symmetry boundary and the parallel side boundary were fixed against the y-axis. For other side planes, nodes at the same depth move together along the loading direction (x-axis) to simulate the free-field condition. For saturated soils, the pore water pressure developed freely at the internal nodes except for nodes at the ground surface. All analyses were carried out in three loading stages: self-weight loading, pile installation loading and dynamic loading. During the second stage, a soil column at the model center was replaced by the pile followed by a monotonic loading analysis due to the self-weight of the pile or superstructure. Finally, a pushover load was applied at the pile top, or a seismic load was applied by accelerating the model along the x-axis. The model was allowed to rest for several seconds after loading.

2.2 *Soil-pile system modelling*

Parameters for the PDMY02 material adopted in the following simulations are presented in Table 1. Some of them, such as relative density D_r, saturated density ρ, void ratio e, shear modulus G_r, and bulk modulus B_r, were derived from the measured values of corresponding experiments (i.e. Zhang et al. 1999, Wilson 1998). Friction angle φ_f and permeability coefficient k of Nevada sand were selected from Choobbasti & Zahmatkesh (2016). Other parameters were suggested by the material manual (Mazzoni et al. 2007). The pile was simulated by employing elastic beam column elements. A series of stiff elastic beam elements (rigid links) was used as "connections" between pile and soil nodes as suggested by Cheng & Jeremić (2009). Pile nodes and rigid link nodes were bonded to move translationally and rotationally together. These rigid links were able to shape the pile geometry and prevent the soil opening from collapsing.

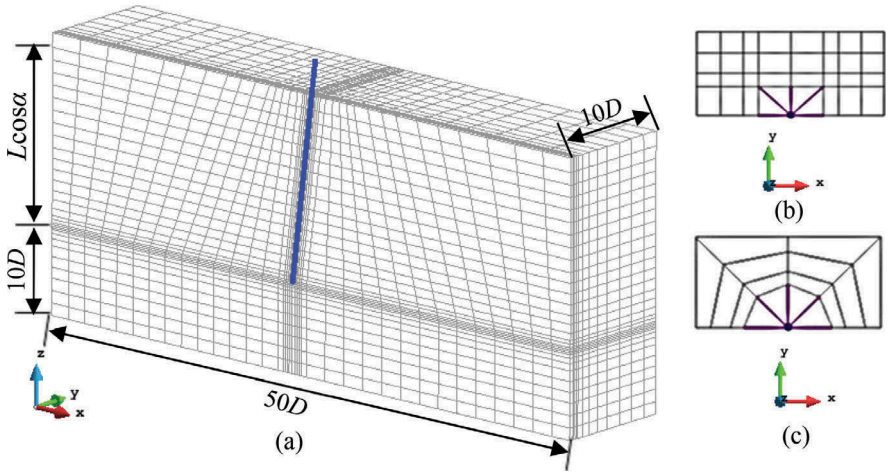

Figure 1. Typical schematic for the 3D FEM analyses: (a) model layout; (b) mesh for the square pile; and (c) mesh for the circular pile.

Table 1. PDMY02 material parameters.

Material parameters	Edgar-Allen Sand	Nevada Sand	
Relative density D_r (%)	55	80	55
Saturated soil mass density ρ (ton/m^3)	1.92	2.03	2.02
Reference effective confining pressure p_r (kPa)	101	101	101
Reference shear modulus G_r (MPa)	86.25	115.0	101.2
Reference bulk modulus B_r (MPa)	186.9	249.1	219.2
Friction angle φ_f (°)	37.1	39.5	35.0
Pressure dependency coefficient d	0.5	0.5	0.5
Phase transformation angle φ_{PT} (°)	26.0	26.0	26.0
Contraction coefficient c_1	0.037	0.013	0.037
Contraction coefficient c_2	5.0	5.0	5.0
Contraction coefficient c_3	0.1	0.0	0.1
Dilation coefficient d_1	0.08	0.3	0.08
Dilation coefficient d_2	3.0	3.0	3.0
Dilation coefficient d_3	0.1	0.0	0.1
Liquefaction-induced strain constants (liq_1, liq_2)	1.0, 0.0	1.0, 0.0	1.0, 0.0
Peak shear strain γ_{max}	0.1	0.1	0.1
Number of yield surface	20	20	20
Void ratio e	0.780	0.594	0.681
Permeability coefficient k (m/s)	-	3.70×10^{-5}	6.05×10^{-5}

In order to simulate the friction and separation mechanisms at the soil-pile interface, zero-length flat slider bearing elements (Mazzoni et al. 2007) with conventional Coulomb friction properties were inserted between the rigid links and the surrounding soil elements. Zero cohesive strength was considered, and the friction coefficient was taken as $\tan(2\varphi_f/3)$ in which φ_f is the friction angle of the surrounding soil. Based on Kolay et al. (2013) and some parametric studies, values of the normal (K_N) and tangential (K_T) stiffness were set to 1.0×10^7 kPa/m.

3 MODEL VERIFICATION

3.1 *Inclined pile subject to monotonic loading*

In the centrifuge experiment of Zhang et al. (1999), single square inclined piles with different inclinations were inserted in a medium-dense (D_r = 55%) dry Edgar-Allen sand. Width D and embedment length of the pile were 0.43 m and 10.9 m, respectively. With different free lengths (2.54 m for the vertical pile and 2.29 m for inclined piles), monotonic pushover loads were applied on the pile head along the x-axis. The section bending stiffness of the pile was EI = 206 MN·m^2 (with E the elastic modulus and I the moment of inertia of the pile). G_r was calculated on the following relation (Das & Ramana 2011):

$$G_r = \frac{3230(2.97 - e)^2}{1 + e} p_r^{0.5} \tag{1}$$

where the void ratio e and reference effective confining pressure p_r were from Table 1. By taking the Poisson's ratio v as 0.3, B_r could be evaluated as:

$$B_r = \frac{2G_r(1 + \upsilon)}{3(1 - 2\upsilon)} \tag{2}$$

The comparisons of the load-displacement curves between numerical and experimental results are shown in Figure 2. The simulated results were reasonably consistent with the experimental results from Zhang et al. (1999).

3.2 *Vertical pile subject to dynamic loading*

For the dynamic behavior, a single vertical pile was modelled, and the results were compared with the centrifuge experiment data (Csp3-J) of Wilson (1998). At prototype scale, an aluminum pipe (EI = 144 MN·m^2) with an outer diameter of 0.67 m and a wall thickness of 0.019 m was installed into a layered saturated Nevada sand stratum. The material parameters for Nevada sand are listed in Table 1 including G_r and B_r calculated by Eq. (1) and Eq. (2), respectively. The upper layer (D_r = 55%) was 9.3 m thick, and the sublayer (D_r = 80%) was 11.4 m thick and extended 3.9 m below the pile toe. A superstructure weighing 49.1 ton was attached to the pile head, at 3.8 m above the ground surface (water table). The 1995 Kobe earthquake acceleration record (Figure 3a) was scaled to 0.22g as the input motion along the x-axis.

The simulation results including excess pore water pressure (EPWP) and pile behavior were compared with the centrifuge results in Figure 3b-e. The EPWP was derived from 4.5 m depth below the soil surface. The pile behavior includes the bending moment time history at 0.76 m depth and the acceleration and displacement time histories of the superstructure (SS). Numerical results and experimental data match reasonably well.

4 PARAMETRIC ANALYSIS

The verified modelling method (i.e. the PDMY02 material for the soil, elastic beams for the pile, and interface elements for the soil-pile interaction) has been adopted to investigate the seismic behavior of 2 × 1 pile group configurations with different pile inclinations in saturated sand stratum. Figure 4 presents the model layout with α = 15°. Batter angles ranging from 5 ~ 20° were considered, and the vertical pile group was used as a reference. The pile properties (D = 0.72 m, EI = 505 MN·m^2) and pile group configurations were derived from Li et al. (2016). The pile spaces (center to center) at the soil surface (water level) for different configurations were set as 4D. The pile heads were connected by two rigid links with a concentrated mass of 100 ton in the middle to simulate the cap which was 1.0 m above the soil surface to avoid soil-cap interaction. Material parameters for the Nevada sand in Table 1 were adopted for the two soil layers. The dense (D_r = 80%) and medium-dense (D_r = 55%) layers were 14.0 m and 8.0 m thick, respectively. The Kobe earthquake motion (Figure 3a) was scaled to 0.1g, 0.3g, and 0.4g as input.

4.1 *Soil response*

The maximum excess pore water pressure ratio (r_u) at different soil depths under the cap node (from point A to B) was illustrated in Figure 5. The influence of α is more obvious under higher amplitudes. The maximum r_u at the shallow depth decreases with larger α regardless of amplitudes. With a lower amplitude (Figure 5a), the soil has not liquefied, and α has tiny effects on the maximum r_u in the deep soil layer. However, liquefaction has been observed under higher amplitudes,

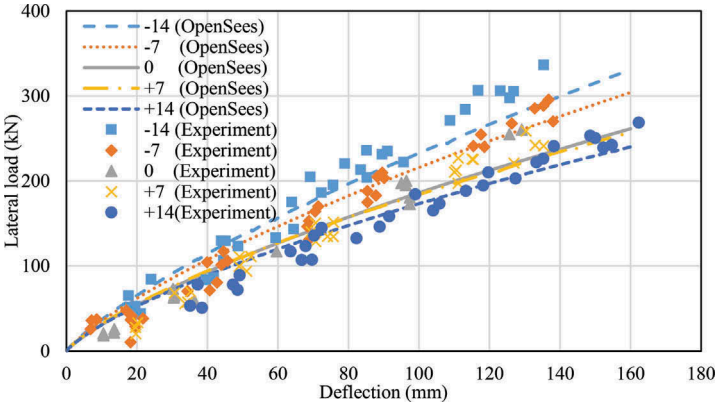

Figure 2. Load-deflection relationships for inclined piles in Edgar-Allen sand.

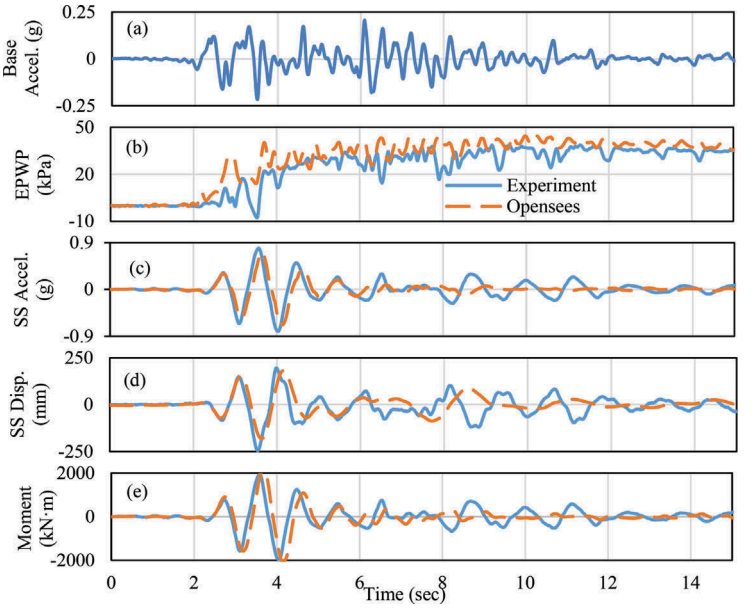

Figure 3. Comparison between numerical and experimental results: (a) base acceleration; (b) EPWP at 4.5 m depth; (c) SS acceleration; (d) SS displacement; (e) bending moment at 0.76 m depth.

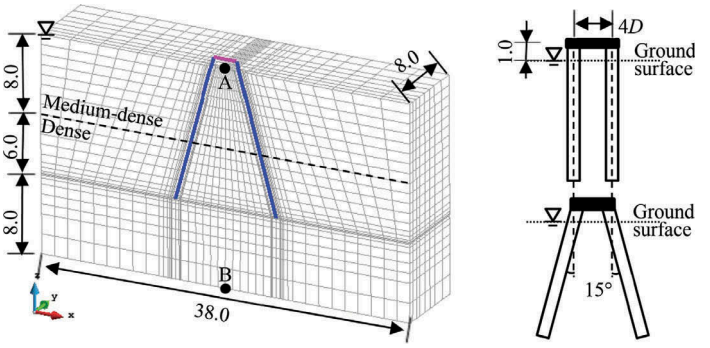

Figure 4. Layout of the numerical model in the parametric analysis (in meters).

and the maximum r_u increases with larger α despite some small reductions near the surface. Therefore, pile inclination promotes pore water pressure development for the liquefied cases. This may be due to the more intensive pile responses which will be investigated subsequently.

4.2 *Cap response*

Based on Li et al. (2016), a performance index P (in percentage) was adopted to evaluate the influence of α quantitatively:

$$P = \frac{Q_{\max,I} - Q_{\max,V}}{Q_{\max,V}} \tag{3}$$

where $Q_{max,I}$ and $Q_{max,V}$ are the calculated quantities for inclined and vertical pile configurations, respectively. Therefore, a positive or negative value of P can reflect the increase or decrease in the concerned quantity due to pile inclination.

For the cap response, attention has been paid on the maximum inertial force ($m_{cap}a_{max}$, with m_{cap} the mass of the cap and a_{max} the maximum acceleration) and lateral displacement.

Figure 6 presents the performance indices for maximum inertial force P_F and lateral displacement $P_{disp,cap}$. All indices are negative which means that pile inclination shows beneficial effects on reducing the inertial force and lateral displacement of the cap. Under the same excitation amplitude, this beneficial effect is getting more significant with the increase in α for all situations, except for the 0.3g and 0.4g excitation cases in Figure 6a. For these two liquefied cases, P_F for 20° inclination is less than that of 15° inclination which means that 15° seems to be an optimum inclination as to the inertial force of the cap. The excitation amplitude indicating the liquefaction depth is not influential on the $P_{disp,cap}$. However, differences of P_F between the non-liquefied case and liquefied cases will be very obvious for lower inclinations.

4.3 *Pile response*

The performance indices for maximum bending moment P_M, maximum shear P_S and axial forces P_A were investigated. Firstly, the distribution of bending moment M along the pile is illustrated in Figure 7. As the left and right piles in the numerical model have similar distributions, only the results of the right pile are presented. There are generally two turning points along the curves for the vertical piles. As α increases, there will be another turning point generated at the shallow depth, and the bending moment at the pile head is also reduced. This investigation is in accordance with the observations of the centrifuge experiments of Li et al. (2016). It is also noteworthy that the locations of all the turning points also move down with the increase in α and the excitation amplitude. Therefore, the maximum bending moment for larger inclinations and excitation amplitudes is not located at the pile head.

As shown in Figure 8a, α mainly plays a beneficial role regarding the bending moment as P_M is in the range of -20 ~ 3%. Although the pile inclination is detrimental in liquefied cases, P_M is less than 3%. Similar properties can be found for P_S shown in Figure 8b except that α exhibits significant detrimental effects in the liquefied cases with P_S in the range of 15 ~ 45%.

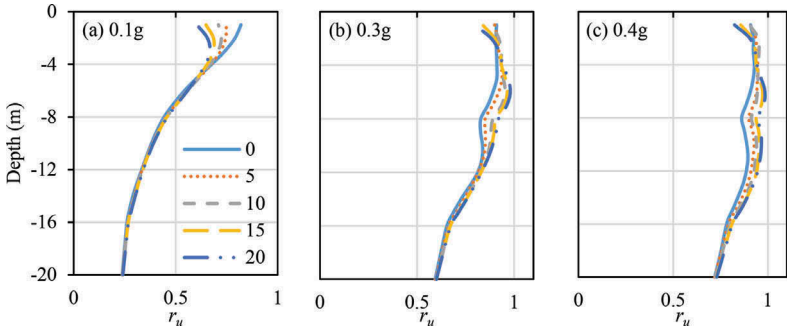

Figure 5. Comparison of maximum r_u for different batter angles subjected to various excitation amplitudes: (a) 0.1g; (b) 0.3g; and (c) 0.4g.

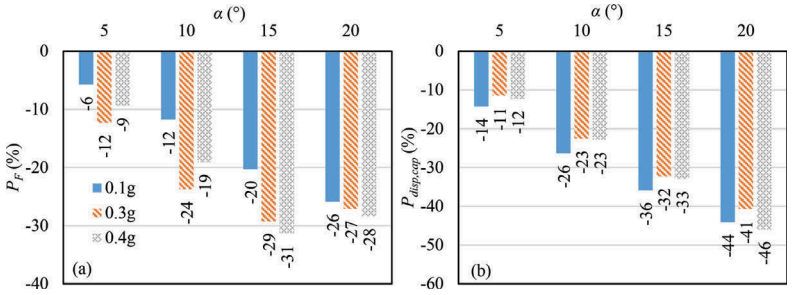

Figure 6. Performance index for the cap response: (a) maximum inertial force P_F; and (b) maximum lateral displacement $P_{disp,cap}$.

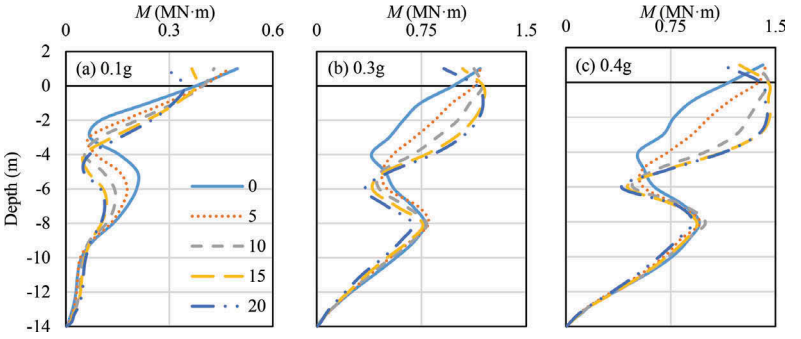

Figure 7. Distribution of bending moment M along the pile subjected to various excitation amplitudes: (a) 0.1g; (b) 0.3g; and (c) 0.4g.

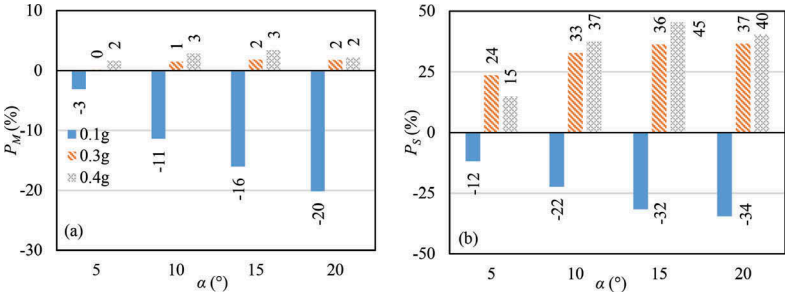

Figure 8. Performance index for the pile response (a) maximum bending moment P_M; and (b) maximum shear force P_S.

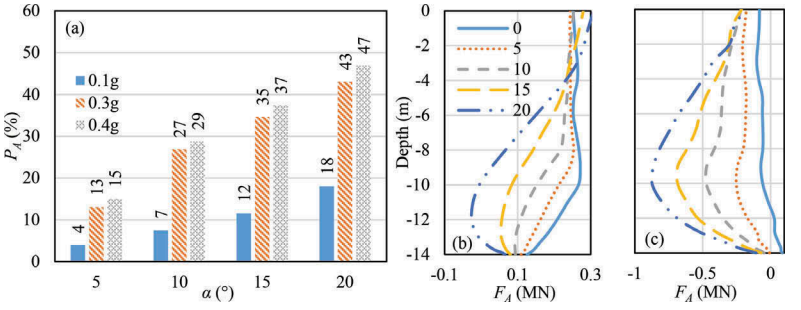

Figure 9. Axial force along the pile: (a) performance index for maximum axial force P_A; and distribution of minimum axial force F_A along the pile subject to various excitation amplitudes: (b) 0.1g and (c) 0.3g.

In terms of P_A, attention should be paid as negative forces (tension) may be generated during the seismic loading. As illustrated in Figure 9a, pile inclination is detrimental for all cases. For the non-liquefied case, this detrimental effect is not violent as P_A is in the range of 4 ~ 18%. As the soil liquefies, P_A increases significantly to 13 ~ 47%. The distribution of minimum axial force F_A (Figure 9b, c) shows that negative F_A has been generated and an extensive increase can be observed for cases with larger amplitudes and pile inclinations.

5 CONCLUSIONS

This research proposes a 3D FEM model using the OpenSees platform to investigate the seismic behavior of the soil-pile system in liquefiable sands. The primary outcomes are as follows:

- Soil response: pile inclination impeded the development of EPWP at a shallow depth. However, it motivated the EPWP development as the soil liquefied.
- Cap response: pile inclination was beneficial in reducing the maximum inertial force (with P_F down to -31%) and lateral displacement (with $P_{disp,cap}$ down to -46%) of the cap in both liquefied and non-liquefied cases.
- Pile response: pile inclination had a beneficial effect (negative performance index) on the bending moment (with P_M down to -20%) and shear force (with P_S down to -34%) for non-liquefied cases. However, detrimental effects (positive performance index) have been detected as the soil liquefies. Besides, piles with larger inclinations induced higher axial forces (both compression and tension forces).

Overall, the application of inclined piles could produce better performance for the soil-pile-cap system in non-liquefied soils. With the influence of soil liquefaction, this beneficial effect turned detrimental to the response of the soil-pile system, except to the cap response.

REFERENCES

Berrill, J.B., Christensen, S.A., Keenan, R.P., et al. 2001. Case study of lateral spreading forces on a piled foundation. *Géotechnique* 51(6): 501–517.

Cheng, Z. & Jeremić, B. 2009. Numerical modeling and simulation of pile in liquefiable soil. *Soil Dynamics and Earthquake Engineering* 29(11–12): 1405–1416.

Choobbasti, A.J. & Zahmatkesh, A. 2016. Computation of degradation factors of py curves in liquefiable soils for analysis of piles using three-dimensional finite-element model. *Soil Dynamics and Earthquake Engineering* 89: 61-74.

Das, B.M. & Ramana, G.V. 2011. *Principles of Soil Dynamics (2nd Edition)*. Stamford: Cengage Learning.

Dash, S.R. & Bhattacharya, S. 2015. Pore water pressure generation and dissipation near to pile and far-field in liquefiable soils. *International Journal of GEOMATE: Geotechnique, Construction Materials and Environment* 9(1): 1454–1459.

Elgamal, A., Yang, Z., Parra, E., et al. 2003. Modeling of cyclic mobility in saturated cohesionless soils. *International Journal of Plasticity* 19(6): 883-905.

Escoffier, S. 2012. Experimental study of the effect of inclined pile on the seismic behavior of pile group. *Soil Dynamics and Earthquake Engineering* 42: 275–291.

Gerolymos, N. Giannakou, A., Anastasopoulos, I., et al. 2008. Evidence of beneficial role of inclined piles: Observations and summary of numerical analyses. *Bulletin of Earthquake Engineering* 6(4): 705–722.

Ghorbani, A., Hasanzadehshooiili, H., Ghamari, E., et al. 2014. Comprehensive three dimensional finite element analysis, parametric study and sensitivity analysis on the seismic performance of soil-micropile-superstructure interaction. *Soil Dynamics and Earthquake Engineering* 58: 21–36.

Goit, C.S. & Saitoh, M. 2013. Model tests and numerical analyses on horizontal impedance functions of inclined single piles embedded in cohesionless soil. *Earthquake Engineering and Engineering Vibration* 12 (1): 143–154.

Kolay, C., Prashant, A. & Jain, S.K. 2013. Nonlinear dynamic analysis and seismic coefficient for abutments and retaining walls. *Earthquake Spectra* 29(2): 427–451.

Li, Z., Escoffier, S. & Kotronis, P. 2016. Centrifuge modeling of batter pile foundations under earthquake excitation. *Soil Dynamics and Earthquake Engineering* 88: 176–190.

Mazzoni, S, McKenna, F., Scott, M.H., et al. 2007. *OpenSees command language manual*. Pacific Earthquake Engineering Research (PEER) Center.

McManus, K., Turner, J.P. & Charton, G. 2005. Inclined reinforcement to prevent soil liquefaction. In *Proceedings of the Annual NZSEE Technical Conference*. Wairakei, New Zealand.

Pender, M. 1993. Aseismic pile foundation design analysis. *Bulletin of the New Zealand National Society for Earthquake Engineering* 26(1): 49–160.

Wang, S. & Orense, R.P. 2014. Modelling of raked pile foundations in liquefiable ground. *Soil Dynamics and Earthquake Engineering* 64: 11–23.

Wilson, D.W. 1998. Soil-pile-superstructure interaction in liquefying sand and soft clay. *PhD Thesis*, University of California, Davis.

Zhang, L., McVay, M.C. & Lai, P.W. 1999. Centrifuge modelling of laterally loaded single battered piles in sands. *Canadian Geotechnical Journal* 36(6): 1074–1084.